An upgraded x-ray spectroscopy diagnostic on MST[a)]

D. J. Clayton,[b)] A. F. Almagri, D. R. Burke, C. B. Forest, J. A. Goetz, M. C. Kaufman, and R. O'Connell
Department of Physics, University of Wisconsin-Madison, Madison, Wisconsin 53706, USA

(Presented 19 May 2010; received 13 May 2010; accepted 27 June 2010; published online 7 October 2010)

An upgraded x-ray spectroscopy diagnostic is used to measure the distribution of fast electrons in MST and to determine Z_{eff} and the particle diffusion coefficient D_r. A radial array of 12 CdZnTe hard-x-ray detectors measures 10–150 keV Bremsstrahlung from fast electrons, a signature of reduced stochasticity and improved confinement in the plasma. A new Si soft-x-ray detector measures 2–10 keV Bremsstrahlung from thermal and fast electrons. The shaped output pulses from both detector types are digitized and the resulting waveforms are fit with Gaussians to resolve pileup and provide good time and energy resolution. Lead apertures prevent detector saturation and provide a well-known etendue, while lead shielding prevents pickup from stray x-rays. New Be vacuum windows transmit >2 keV x-rays, and additional Al and Be filters are sometimes used to reduce low energy flux for better resolution at higher energies. Measured spectra are compared to those predicted by the Fokker–Planck code CQL3D to deduce Z_{eff} and D_r. © *2010 American Institute of Physics.* [doi:10.1063/1.3478977]

I. INTRODUCTION

A radially resolved x-ray spectroscopy diagnostic is installed on the Madison Symmetric Torus (MST) (Ref. 1) reversed-field pinch to measure fast electron transport via emitted Bremsstrahlung, a technique previously used on other toroidal devices such as JET.[2] During standard MST discharges, current-driven tearing modes create stochastic magnetic fields that dominate particle transport; fast electrons diffuse radially at a rate proportional to their velocity.[3] In these discharges, fast electrons are quickly lost from the core of the plasma and no x-rays above 10 keV are detected. When stochasticity is reduced, either by inductive current profile modification or by the formation of a single large island, fast electrons are better confined and x-rays with energies up to 150 keV are observed.[4,5] In some cases, modeling with the Fokker–Planck code CQL3D (Ref. 6) enables the radial diffusion rate D_r and the effective ion charge Z_{eff} to be inferred from the measured x-ray spectra.

Hard-x-ray Bremsstrahlung from fast electrons is measured by an array of CdZnTe photodiode detectors. Soft-x-ray Bremsstrahlung from thermal and fast electrons is measured by a silicon detector. CdZnTe and Si semiconductor detectors were selected for their fast response time, excellent energy resolution, and room-temperature operation.[7] The CdZnTe detectors have an energy resolution of about 2 keV and the Si detector has a resolution of 0.45 keV. These detectors are run in a pulse mode to enable spectroscopic measurements. Rather than using conventional pulse height analysis, the signals from each detector are fully digitized and stored for later processing. A fitting routine assigns an arrival time and x-ray energy to each detected pulse, allowing for the study of fast dynamic processes. Pulses can be sorted into useful time and energy bins to best suit a particular analysis. Other advantages of digitizing the signals include the ability to separate Gaussian pulses from noise and identifying, and possibly resolving, the pileup of pulses. With the proper apertures and filters, spectra can be found from a 1 ms time slice with a radial resolution of 5 cm.

II. DESCRIPTION OF THE DIAGNOSTIC

A. X-ray detectors

The diagnostic consists of a set of individually packaged single-crystal photodiode detectors. Twelve CdZnTe hard-x-ray (hxr) detectors were custom-built for MST by eV Products (now EI Detection & Imaging Systems, a division of Endicott Interconnect Technologies, Inc.).[8] The $10\times10\times2$ mm^3 CdZnTe crystals are thinner than their off-the-shelf counterparts, maximizing their energy resolution while maintaining a high detection efficiency in the 10–150 keV energy range for which they are used. Each photodiode is packaged with a charge-sensitive preamplifier, making the total unit $52\times20\times14$ mm^3. Included in the system is a power supply that provides the bias voltage and preamp power for each detector.

In addition to the hxr detectors, an XR-100CR detector from Amptek Inc. is used to measure lower energy soft-x-rays (sxr). This detector has a maximum efficiency in the 2–10 keV energy range. The unit includes a Si photodiode, charge-sensitive preamplifier, and thermoelectric cooler with monitor to regulate the photodiode's temperature. The detector crystal measures $5.0\times5.0\times0.5$ mm^3 and the total package is $83\times57\times28$ mm^3. Amptek PC5 power supplies provide the bias voltage, preamp power, and thermoelectric

[a)]Contributed paper, published as part of the Proceedings of the 18th Topical Conference on High-Temperature Plasma Diagnostics, Wildwood, New Jersey, May 2010.
[b)]Electronic mail: dclayton@pppl.gov.

 © 2010 American Institute of Physics

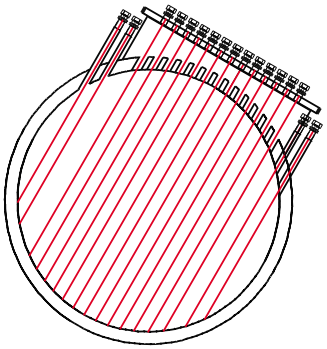

FIG. 1. (Color online) The lines of sight of the radial array.

cooling power. Five more of these off-the-shelf detectors are currently being added to the diagnostic to provide radial profile measurements in this energy range.

The signals from the detectors are further amplified by pulse shaping amplifiers, which increase the magnitude of the pulses, reduce the noise of the signal, and provide a quickly restored baseline to allow for higher counting rates. For this diagnostic, Gaussian shaping amplifiers were selected to provide pulses that are easily fit after digitization; the heights of the Gaussian pulses are proportional to x-ray energy and the amplifier gain can be adjusted to produce pulse heights appropriate for the ± 5 V digitizer inputs. The shaping amplifiers provided by eV Products produce pulses with a full width at half maximum (FWHM) of 1.2 μs. Shaping amplifiers for the Amptek detectors are from Cremat, Inc. Two sets of amplifiers are used: one produces pulses with FWHM of 1.2 μs, the same as the hxr amplifiers, and the other provides 240 ns pulses, for improved time resolution.

B. Detector installation

An advantage of using small photodiode detectors is that they are relatively easy to move. Twenty-five x-ray windows are currently installed on MST and a detector can be moved from one window to another in less than a minute. The majority of the x-ray detectors are distributed along a radial array of 17 windows spaced 2 in. apart, covering a radial range of roughly $r/a = \pm 0.8$, as shown in Fig. 1. Eight additional windows are installed at other various toroidal locations.

The previous aluminum x-ray windows have recently been replaced with 150 μm beryllium windows to allow transmission of sxrs. The detectors are mounted above the windows using Sorbothane®, a vibration-damping material that reduces mechanical vibrations that otherwise create noise in the detector signals. The hxr detectors are encased in lead boxes to eliminate the pickup of stray x-rays that escape the vacuum vessel. The sxr detector must be wrapped in aluminum foil to shield it from electromagnetic noise.

C. Signal processing

The amplified signals are recorded by two Hytec VTR 2535W eight-channel VME analog-to-digital converters. These digitizers convert ± 5 V input signals into 12 bit, 10 Msample per second data. Each channel can record up to 524 ksamples per discharge. These digitizers are currently being replaced by three Struck SIS3302 eight-channel VME ACDs. Each channel will have 16-bit resolution and will record up to 100 Msamples per second, storing 32 Msamples per channel. Besides providing additional channels to accommodate the new sxr array, these new digitizers will allow fitting to the shorter 240 ns Cremat shaping amplifier pulses.

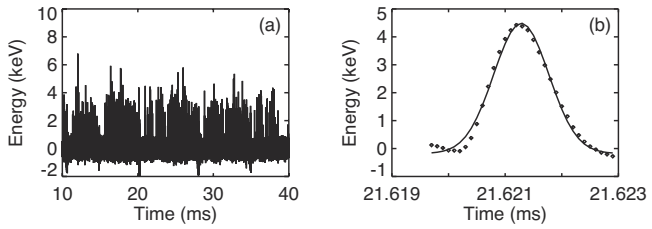

FIG. 2. (a) Digitized signal from the Si detector during a 400 kA MST discharge. (b) A closeup of a pulse fit with a Gaussian at 21.6213 ms, found to have an energy of 4.67 keV.

Once the digitized signal is stored and transferred to a hard drive, a fitting routine picks out pulses and records their heights and arrival times. A Gaussian of fixed width is fit to each pulse, as shown in Fig. 2. If the chi square of the fit exceeds a set threshold, an attempt is then made to fit two overlapping Gaussians to the pulse. If this also fails, the pulse is rejected as pileup or noise, though this is also recorded to provide a measure of the quality of the final data set.

Energy calibration is performed with known x-ray sources. Before calibration, the voltage gain on each shaping amplifier is adjusted to utilize the full 5 V range of the digitizers. Thousands of pulses are then measured from the source and the mean and standard deviations of all the pulse heights provide the proper bit value to x-ray energy calibration and the error in the energy measurement, respectively. Typical errors are 450 eV for the sxr detectors and 2 keV for the hxr detectors. Once this is complete, an energy can be assigned to every pulse measured during a plasma discharge. The final output of the fitting routine after each discharge is a three-columned array that assigns a time, energy, and detector number to every x-ray measured.

D. Calculating energy flux and spectra

After the pulses are fit and calibrated, they can be binned by time and energy to produce spectra. The primary source of error in the resulting spectra is the finite count rate. Since only continuous emission is of interest with this diagnostic, about 100 counts are enough to provide an adequate spectrum. These 100 counts can be collected in about 1 ms when using 1.2 μs pulses, or in 200 μs with 240 ns pulse widths. Once binned, the resulting data represent the total energy collected by each detector in each time and energy window. These data must then be normalized by the bin size, the detector viewing geometry as determined by a set of apertures, and the filter transmission to produce a flux that can be compared to other experiments or computations. These normalized data are expressed in units of ergs $\mathrm{cm}^{-2}\ \mathrm{sr}^{-1}\ \mathrm{s}^{-1}\ \mathrm{keV}^{-1}$.

Apertures are used to limit the x-ray flux that reaches a detector to prevent pulse pileup. Depending on MST plasma conditions, x-ray flux can vary by many orders of magnitude, thus several aperture sizes and configurations are needed to prevent pileup while still allowing enough flux through for an accurate measurement. Each detector has two apertures spaced 2 or 4 in. apart, each aperture with a diameter between 0.05 and 0.15 in. These apertures are made from 6 mm thick lead in the case of the hxr detectors and 6 mm thick aluminum in the sxr case; these materials effectively block all x-rays from outside the expected detector view. The measured energy flux is divided by etendue, the detection area times the solid angle viewed, for a result that is independent of the apertures used.

To improve flux resolution at higher energies, 300 μm and 1 mm beryllium filters are sometimes used with the sxr detector to block low energy x-rays. When placing the hxr detectors on the new beryllium windows, aluminum filters must be used to prevent sxrs from saturating the signal. 250 μm, 400 μm, and 4 mm aluminum filters are available. To properly normalize the data, each bin must be divided by the transmission of the filter. Since transmission is a function of energy, the energy bins must be narrow enough to have a well-defined transmission, but wide enough for good count rates. For data that are presented as a sum over all energies, the pulses were first separated into small energy bins, each bin was divided by the appropriate transmission, and then the bins were summed together.

III. EXAMPLES OF MEASUREMENTS

Examples of measurements from the diagnostic are provided in Fig. 3. In Fig. 3(a), hxr flux measured along the central line of sight is plotted versus time for a 400 kA MST discharge with pulsed parallel current drive (PPCD),[9] where the current profile is inductively modified to reduce tearing mode amplitudes and thus reduce stochasticity. X-ray flux grows exponentially during the first few milliseconds of PPCD, saturates, then quickly dissipates as PPCD ends and stochasticity returns. The radial profile of line-integrated hxr flux during this discharge is peaked in the core, as seen in Fig. 3(b). This is compared to another discharge during which a single, large, magnetic island spontaneously forms in the plasma.[5] In this case, fast electrons are generated within the island, then diffuse stochastically throughout the plasma volume, creating a much flatter radial profile. Figure 3(c) compares spectra measured during a 550 kA PPCD discharge by the Si detector and a CdZnTe detector, both with lines of sight through the magnetic axis. In Fig. 3(d), the sxr spectrum measured during a 400 kA PPCD discharge is compared to expected spectra calculated using CQL3D. In this case, CQL3D runs with D_r=5.0 m^2/s and Z_{eff}=5 give the best fit to the measured spectrum. The addition of the new sxr detectors will provide spectra that may be used with CQL3D to infer the radial profiles of D_r and Z_{eff}, and the newly improved time resolution of the diagnostic will be used to study energetic electron transport during fast processes, such as the sudden crash of hxr flux at the end of PPCD.

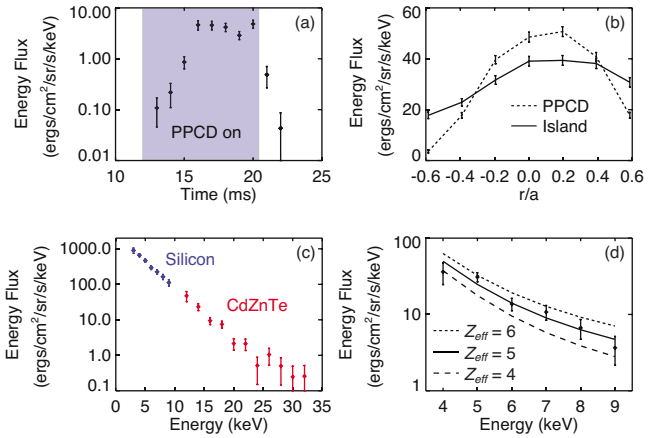

FIG. 3. (Color online) (a) Hard-x-ray flux vs time measured by the central chord during a 400 kA PPCD discharge. Tearing mode amplitudes are reduced during the shaded time. (b) A comparison of line-integrated hxr flux radial profiles between a 400 kA discharge with PPCD and a 400 kA discharge with a magnetic island. (c) X-ray spectra measured by the Si detector and the central CdZnTe detector during a 550 kA PPCD discharge. (d) Soft-x-ray spectrum from a 400 kA PPCD discharge compared to CQL3D predictions for D_r=5 m^2/s and Z_{eff}=4–6.

[1] R. N. Dexter, D. W. Kerst, T. W. Lovell, S. C. Prager, and J. C. Sprott, Fusion Technol. **19**, 131 (1991).
[2] B. Esposito, R. M. Solis, P. van Belle, O. N. Jarvis, F. B. Marcus, G. Sadler, R. Sanchez, B. Fischer, P. Froissard, J. M. Adams, E. Cecil, and N. Watkins, Plasma Phys. Controlled Fusion **38**, 2035 (1996).
[3] A. B. Rechester and M. N. Rosenbluth, Phys. Rev. Lett. **40**, 38 (1978).
[4] R. O'Connell, D. J. Den Hartog, C. B. Forest, J. K. Anderson, T. M. Biewer, B. E. Chapman, D. Craig, G. Fiksel, S. C. Prager, J. S. Sarff, and S. D. Terry, Phys. Rev. Lett. **91**, 045002 (2003).
[5] D. J. Clayton, B. E. Chapman, R. O'Connell, A. F. Almagri, D. R. Burke, C. B. Forest, J. A. Goetz, M. C. Kaufman, F. Bonomo, P. Franz, M. Gobbin, and P. Piovesan, Phys. Plasmas **17**, 012505 (2010).
[6] R. W. Harvey and M. G. McCoy, *Proceedings of the IAEA TCM on Advances in Simulation and Modeling of Thermonuclear Plasmas*, Montreal, 1992 (IAEA, Vienna, 1993), pp. 489–526.
[7] Y. Peysson and R. Arslanbekov, Nucl. Instrum. Methods Phys. Res. A **380**, 423 (1996).
[8] R. O'Connell, D. J. D. Hartog, C. B. Forest, and R. W. Harvey, Rev. Sci. Instrum. **74**, 2001 (2003).
[9] J. S. Sarff, S. A. Hokin, H. Ji, S. C. Prager, and C. R. Sovinec, Phys. Rev. Lett. **72**, 3670 (1994).